JACS
JOURNAL OF THE AMERICAN CHEMICAL SOCIETY
Communication
pubs.acs.org/JACS

Air-Stable Surface Charge Transfer Doping of MoS_2 by Benzyl Viologen

Daisuke Kiriya,[†,‡,§] Mahmut Tosun,[†,‡,§] Peida Zhao,[†,‡,§] Jeong Seuk Kang,[†,‡] and Ali Javey*[,†,‡,§]

[†]Electrical Engineering and Computer Sciences, University of California, Berkeley, California 94720, United States
[‡]Materials Sciences Division, Lawrence Berkeley National Laboratory, Berkeley, California 94720, United States
[§]Berkeley Sensor and Actuator Center, University of California, Berkeley, California 94720, United States

Supporting Information

ABSTRACT: Air-stable doping of transition metal dichalcogenides is of fundamental importance to enable a wide range of optoelectronic and electronic devices while exploring their basic material properties. Here we demonstrate the use of benzyl viologen (BV), which has one of the highest reduction potentials of all electron-donor organic compounds, as a surface charge transfer donor for MoS_2 flakes. The n-doped samples exhibit excellent stability in both ambient air and vacuum. Notably, we obtained a high electron sheet density of $\sim 1.2 \times 10^{13}$ cm^{-2}, which corresponds to the degenerate doping limit for MoS_2. The BV dopant molecules can be reversibly removed by immersion in toluene, providing the ability to control the carrier sheet density as well as selective removal of surface dopants on demand. By BV doping of MoS_2 at the metal junctions, the contact resistances are shown to be reduced by a factor of >3. As a proof of concept, top-gated field-effect transistors were fabricated with BV-doped n^+ source/drain contacts self-aligned with respect to the top gate. The device architecture, resembling that of the conventional Si transistors, exhibited excellent switching characteristics with a subthreshold swing of ~77 mV/decade.

Transition metal dichalcogenides (TMDCs) are a promising class of layered semiconductors exhibiting atomically uniform thicknesses with a wide range of band gaps and band alignments.[1−4] They can be scaled down to a monolayer in thickness, providing a model two-dimensional (2D) material system for exploiting nanoscale phenomena while presenting a promising platform for future electronics and optoelectronics with novel functionalities.[5−9] As in any semiconductor, controlled chemical doping is essential for modulating the carrier concentrations and electronic properties, thereby enabling fabrication of various homo/heterojunctions and complex devices.[3,4,10−12] In this regard, surface charge transfer doping of TMDCs, including MoS_2 and WSe_2, has been demonstrated in the past using surface-adsorbed potassium[12] and NO_2[11] species as donors and acceptors, respectively. This doping concept is similar to what has been previously exploited for other molecular-scale materials such as organic molecules[13] and polymers,[14] carbon nanotubes,[15] graphene,[16] and ultrathin III−V membranes.[17] In this approach, by the choice of surface-adsorbed species with proper reduction potentials with respect to that of the desired semiconductor, either electron donation or electron withdrawal can be induced. Notably, in comparison with conventional substitutional doping, surface charge transfer does not induce defects in the semiconductor lattice. While adsorbed K atoms have been shown to be highly effective in donating electrons to TMDCs for n-type doping, the approach lacks air stability.[12] K atoms vigorously react with ambient air and water molecules, thereby making the process viable only in a high-vacuum environment. In this regard, the development of air-stable dopants for TMDCs is of tremendous interest for further advancement of the field. Here we demonstrate air-stable n-doping of MoS_2 up to the degenerate level using benzyl viologen (BV) as the surface charge transfer donor. BV doping was previously applied to carbon nanostructures, including graphene[18] and nanotubes,[19] demonstrating its stable electron donating characteristics. Here we studied the effectiveness of BV as a donor in few-layer MoS_2 crystals. Electron transfer from the BV molecule to MoS_2 generates an electron transfer complex that is stable under ambient conditions as well as in vacuum, allowing for extensive device and electron transport characterizations as well as facilitating a deeper level of material understanding. As a proof of concept, we show that degenerate n-doping of MoS_2 in the proximity of metal contacts reduces the contact resistance for electron injection by a factor of ~3 as a result of thinning of the Schottky barrier (SB). Furthermore, we fabricated high-performance top-gated MoS_2 transistors in which the gate electrode is used as a self-aligned mask to selectively dope the source/drain regions of MoS_2. The resulting $n^+/i/n^+$ devices resemble conventional n-MOSFETs, exhibiting excellent switching characteristics. The present work introduces a highly stable and effective n-doping scheme for MoS_2 based on a hybrid system of synergistically interactive organic molecules and inorganic TMDCs.

The structure of the dopant molecule BV is shown in Figure 1a. BV has one of the lowest reduction potentials among all electron-donor organic molecules,[20] making it an optimal choice for use as a donor. The neutral BV molecule ($\mathbf{BV^0}$) transfers electrons to an acceptor material (in this case, MoS_2), and eventually a two-electron transfer process is carried out to generate an electron transfer complex between the divalent BV molecule ($\mathbf{BV^{2+}}$) and a divalent acceptor material (acceptor^{2-} state). The energy diagram shown in Figure 1c depicts the

Received: April 8, 2014
Published: May 16, 2014

dx.doi.org/10.1021/ja5033327 | J. Am. Chem. Soc. 2014, 136, 7853−7856

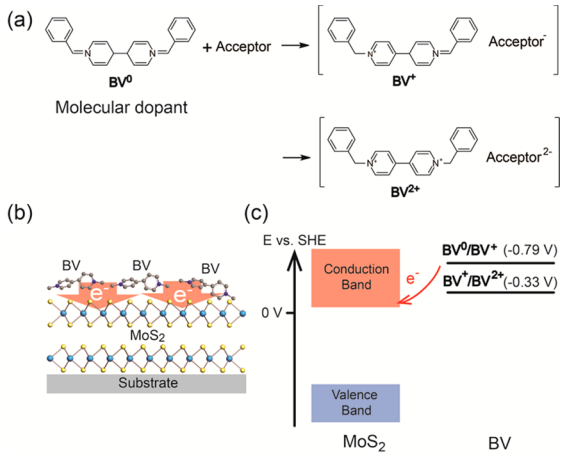

Figure 1. (a) Redox reactions of the BV molecule when it is adsorbed on an acceptor material (in this case, MoS_2). (b) Schematic illustration of BV surface doping of MoS_2. The phenyl rings have been omitted from the schematics of BV molecules for simplification. Color code: C (gray), N (dark blue), Mo (light blue), S (yellow). (c) Energy band diagram of MoS_2 and BV redox states. The conduction band edge of MoS_2 is located at ~0 V vs SHE, which is lower than the redox potentials of the BV molecules. This energy level offset results in electron donation from BV molecules to MoS_2.

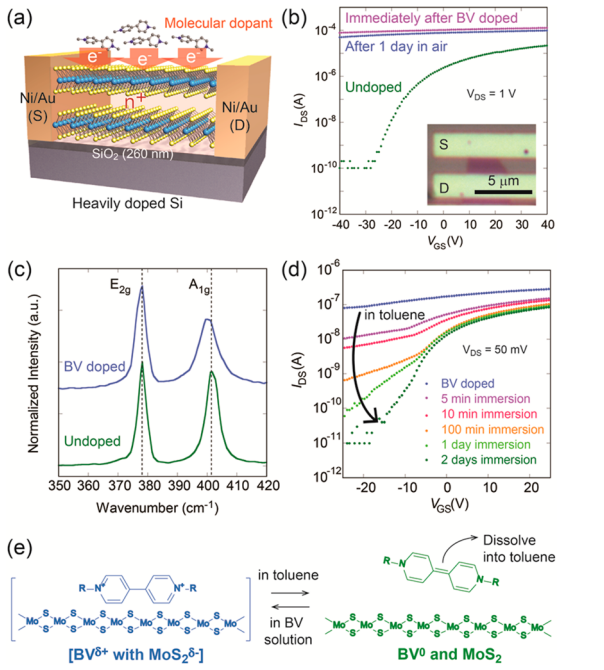

Figure 2. (a) Schematic illustration of a back-gated MoS_2 device used for BV surface charge transfer doping studies. The phenyl rings have been omitted in the schematics of BV molecules for simplification. (b) Transfer characteristic curves of the device before doping (green), right after BV doping (purple), and after the doped device was kept in air for 1 day (blue) at V_{DS} = 1 V. The inset shows an optical microscope image of the device, consisting of trilayer MoS_2. (c) Raman spectra of a trilayer MoS_2 flake before (undoped, green curve) and after BV doping (BV-doped, blue curve). The spectra are normalized to the E_{2g} peaks. (d) Transfer characteristics of a BV-doped device as a function of time of immersion in toluene, depicting the on-demand removal of BV surface dopants. As the BV molecules were dissolved away in toluene, the I_{DS}–V_{GS} curves were converted back to the original characteristic profile. (e) Schematic illustration of the desorption/adsorption of BV molecules from/onto the MoS_2 surface through immersion in neat toluene/BV-containing toluene solution, respectively.

expected energy level offset between the conduction band edge of MoS_2 and the reduction potential of the BV molecule. It has been reported in the literature that MoS_2 has a conduction band edge at around 0 V vs the standard hydrogen electrode (SHE),[5,21,22] while the reduction potentials of the BV molecule are −0.79 V ($\mathbf{BV^0}/\mathbf{BV^+}$) and −0.33 V ($\mathbf{BV^+}/\mathbf{BV^{2+}}$).[19] Because of this energy level offset, MoS_2 acts as an electron-acceptor material, and the $\mathbf{BV^0}$ molecule can readily transfer electrons to MoS_2.

The charge transfer between BV and MoS_2 was experimentally probed through electrical measurements and Raman spectroscopy. For electron characterization, a wide range of device test structures were fabricated. First, back-gated MoS_2 field-effect transistors (FETs) were fabricated (Figure 2a), and the electrical properties were measured before and after BV doping. The back-gated devices were fabricated with standard lithographic techniques using mechanically exfoliated few-layer MoS_2. The MoS_2 was mechanically exfoliated onto a heavily doped (p^+) 260 nm thick Si/SiO_2 substrate, which acted as the global back gate, and 30/30 nm Ni/Au metal stacks were used for the source (S)/drain (D) contacts. A yellow solution of BV in toluene (1–5 mg/mL) was synthesized. The sample was then immersed into the BV solution for 12 h and then dried using N_2 gas [see the Supporting Information (SI) for details]. The transfer characteristics of a representative trilayer MoS_2 device are shown in Figure 2b. The as-made FET showed a strong gate dependence with an on/off current ratio of ~10^5 for applied gate voltages (V_{GS}) ranging from −40 to 40 V and an on-current (I_{DS}) level of ~2×10^{-5} A at a source–drain voltage (V_{DS}) of 1 V (Figure 2b). After doping with the BV molecule, the characteristic curve changed drastically. The gate dependence of the current was nearly diminished for the same V_{GS} range and the on-current level was increased by an order of magnitude ($I_{DS} = 1.3 \times 10^{-4}$ A at V_{GS} = 40 V). The lack of gate dependence and the enhanced current density indicate that the MoS_2 was strongly doped by the BV molecules. The 2D sheet density of electrons in MoS_2 can be extracted as $n_{2D} = (I_{DS}L)/(qWV_{DS}\mu)$, where L and W are the channel length and width, respectively, q is the electron charge, and μ is the field-effect mobility. The electron mobility at V_{DS} = 50 mV was calculated as $\mu = G_m L/(V_{DS}C_{ox}W)$, where $C_{ox} = 1.33 \times 10^{-8}$ F/cm^2 is the gate oxide capacitance obtained from the parallel plate model and $G_m = dI_{DS}/dV_{GS}$ is the transconductance. The extracted values of μ and n_{2D} are 24.7 cm^2 V^{-1} s^{-1} and 1.2×10^{13} cm^{-2}, respectively. The extracted n_{2D} is high and corresponds to the degenerate limit. It is similar to the previously reported value of ~10^{13} cm^{-2} obtained for MoS_2 via doping with K,[12] which is a high-redox alkali metal ion (the K/K^+ reduction potential is −2.93 V vs SHE).[23] Notably, the BV-doped device was highly stable in ambient air with only a minimal change in the transfer characteristics over time, even after 9 days of air exposure (Figure 2b and Figure S1 in the SI). This is in contrast to the K-doped samples, which require preparation and measurements in situ under high vacuum since exposure to air causes immediate oxidation of K.[12,23]

The doped samples were also characterized by Raman spectroscopy (Figure 2c). The original Raman spectrum (before doping with BV) shows lateral (E_{2g}) and vertical (A_{1g}) vibration modes of MoS_2 around 378 and 402 cm^{-1}, respectively. After doping with BV, the A_{1g} peak shifted to a

dx.doi.org/10.1021/ja5033327 | J. Am. Chem. Soc. 2014, 136, 7853–7856

lower wavenumber as a result of the softening of A_{1g} vibrations at high electron concentrations.[24] Furthermore, the full width at half maximum (fwhm) of the A_{1g} peak showed broadening from 5.2 to 8.2 cm^{-1}. On the other hand, the E_{2g} peak remained unchanged. These spectroscopic observations are comparable to those in a previous report of electrostatic doping of MoS_2 by a back-gate potential, where the electron−phonon coupling of the A_{1g} mode was suggested to be stronger than that of the E_{2g} mode.[24]

Uniquely, the BV dopants could be reversibly removed from the surface of MoS_2 by immersion in toluene. After immersion into toluene, the current level decreased monotonically over time and the gate dependence of the channel gradually reappeared; eventually, the curve returned to the original (before doping) state (Figure 2d and Figure S1). As mentioned before, the BV molecule and MoS_2 form an air-stable electron transfer complex (Figure 2e). When the doped sample was immersed in toluene, the dopant molecules gradually desorbed from the surface and dissolved in toluene, and the device properties of the MoS_2 FET were converted back to those of the original state. This presents a unique feature of surface charge transfer doping compared with conventional substitutional doping. Here, the dopants can be selectively removed by using proper solvents, which in principle presents one pathway toward patterned doping where only a section of the surface dopants are removed by using a lithographic mask. Furthermore, the 2D electron density (corresponding to the dopant concentration) can be readily tuned through the time of immersion in toluene (Figure 2d).

To quantify the effect of MoS_2 doping on the metal−MoS_2 junction properties, we extracted the contact resistance using the transfer line method (TLM) before and after doping by BV. Five metal lines were fabricated in a parallel manner along a 5 nm thick MoS_2 flake to make four devices with different channel lengths ($L_1 < L_2 < L_3 < L_4$; Figure 3a,b). The transfer characteristic curves at V_{DS} = 50 mV for the MoS_2 FETs with L ranging from 420 to 2910 nm are shown in Figure 3c. Before BV doping, all of the devices showed large gate dependence with threshold voltages (V_T) of about −12 V. After BV doping, the on current increased and the gate dependence was minimal, as previously observed for the device in Figure 2. The estimated total resistance (R_{total}) corresponds to the sum of the resistances from the channel ($R_{channel}$) and the contacts (R_c), represented as $R_{total} = R_{channel} + 2R_c$. $R_{channel}$ is proportional to the channel length, and thus, $R_{total} = 2R_c$ at $L = 0$. From the y intercept of the plot of R_{total} versus L, we can extract the contact resistance R_c for a given gate voltage (Figure S2). Figure 3d depicts the gate-voltage dependences of R_c extracted from the TLM method both with and without BV doping. The R_c values after the BV doping (1.1 kΩ μm at V_{GS} = 40 V and 1.5 kΩ μm at V_{GS} = 0 V) are a factor of about 3 smaller than that for the original undoped sample at high gate fields (3.3 kΩ μm at $V_{GS} - V_T$ = 53.6 V) and reduced by a factor of >100 at low gate fields (e.g., V_{GS} = 0 V). The reduced contact resistance arises from the SB thinning induced by chemical doping to the degenerate limit, enabling a much higher tunneling current to pass directly through the barrier. This effect was further highlighted by temperature-dependent electrical measurements, where a monotonic increase in the on-current level with decreasing temperature was observed for a BV-doped sample (see Figure S4). Thus, the current in our device was limited by phonon scattering in the MoS_2 channel, which has an inverse relationship to temperature, again demonstrating the formation of Ohmic contacts and dominating tunneling current injection without thermionic emission of charge carriers at the metal contact.[25,26] These results clearly demonstrate the effectiveness of BV doping of MoS_2 and its use in reducing the contact resistance, which often limits the device performance of TMDCs.

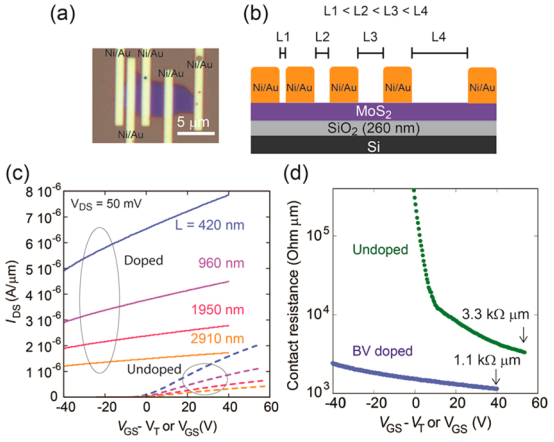

Figure 3. (a) Optical microscope image and (b) schematic of multiple channel length devices fabricated on a single MoS_2 flake to extract the contact resistance using the transmission line model. The flake thickness was ∼5 nm. (c) Transfer characteristic curves of the devices with different channel lengths before (dashed lines) and after (solid lines) BV doping. The data for the device before doping (dashed line) are plotted vs $V_{GS} - V_T$ (V_T = −12 V); on the other hand, the data for the device after the doping are plotted vs V_{GS}. Channel lengths are labeled (420, 960, 1950, and 2910 nm), and the drain voltage used was V_{DS} = 0.05 V. (d) Gate-voltage dependence of the measured contact resistance before (green curve) and after (blue curve) BV doping.

Next, we fabricated a top-gated MoS_2 transistor with underlapped metal contacts (Figures 4a,b and S5). The device had a gate length and width of ∼1.7 and 2.0 μm, respectively. Ni/Au (30/30 nm) metal contacts were used for S/D with Au as the gate electrode and SiO_x/ZrO_2 (1/20 nm) as the gate oxide. The underlapped areas between the top gate and S/D metal contacts (with underlap lengths of 400 and 160 nm on the left and right sides, respectively) were degenerately doped to n^+ using BV molecules to reduce R_c, while the channel masked by the gate remained undoped (i). The gate effectively acted as a self-aligned mask for the fabrication of n^+ contact regions. After BV doping of the top-gated device, the on/off current ratio increased from ∼10^4 to ∼10^6 and the on-current level increased by more than 5 orders of magnitude at V_{DS} = 50 mV (with an increase of more than 2 orders of magnitude at V_{DS} = 1 V; Figure 4c). The subthreshold swing was estimated to be 77 mV/decade after BV doping, which approaches the theoretical limit of 60 mV/decade. The extracted electron mobility was ∼20 cm^2 V^{-1} s^{-1}, which is in the same range as those previously reported for MoS_2 top-gated FETs.[12] The output characteristic curves after BV doping also indicated the small contact resistance of the device (Figures 4d and S5). Furthermore, the environmental stability of this top-gated device was confirmed (Figure S6). These top-gate device results demonstrate the ability to pattern-dope MoS_2 using a room-temperature process, which is needed to enable a wide range of junction-based devices.

To summarize, we have demonstrated highly robust n-doping of MoS_2 crystals with excellent stability in ambient air

dx.doi.org/10.1021/ja5033327 | J. Am. Chem. Soc. 2014, 136, 7853−7856

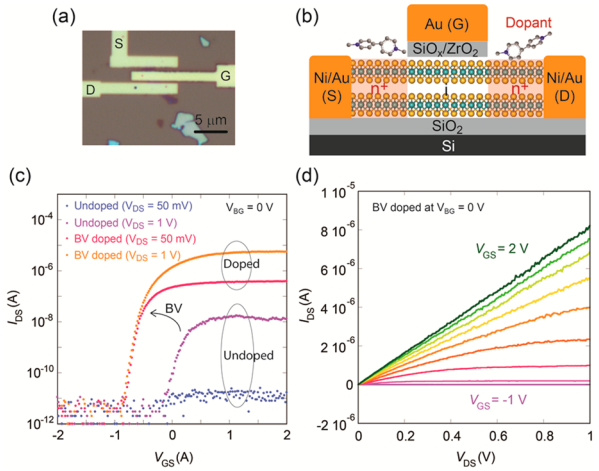

Figure 4. (a) Optical microscope image and (b) schematic of a top-gated MoS_2 device with underlapped regions on each side of the gate. These underlapped regions were doped with BV molecules for the formation of n^+ source/drain contacts, self-aligned with respect to the gate. The device was fabricated from a trilayer MoS_2 flake. (c) Transfer characteristic curves of the top-gate device before (blue and purple) and after (pink and orange) BV treatment at V_{DS} = 50 mV and 1 V. The substrate was grounded during the measurements. (d) Output characteristics of the device after BV doping measured at gate voltage increments of 0.3 V.

and vacuum by using BV, a high-reduction-potential molecule, as the surface charge transfer dopant. The key doping mechanism is surface charge transfer between the dopant BV molecule and MoS_2 to form an electron transfer complex that is air-stable. The BV molecule was able to dope MoS_2 to a high sheet electron density of 1.2×10^{13} cm^{-2}, which we further explored by fabricating a wide range of different transistor structures. In view of the importance of doping control and dopant profiling of semiconductors for exploring various electronic and optoelectronic devices, the ability to pattern-dope TMDCs through an air-stable process presents an important advance in the field that could facilitate probing the intrinsic transport properties of these 2D semiconductors while exploring novel device architectures.

■ ASSOCIATED CONTENT

Ⓢ Supporting Information

Preparation of the BV solution, fabrication and characterization of the devices, temperature dependence of the transfer characteristics, and additional references. This material is available free of charge via the Internet at http://pubs.acs.org.

■ AUTHOR INFORMATION

Corresponding Author

ajavey@berkeley.edu

Notes

The authors declare no competing financial interest.

■ ACKNOWLEDGMENTS

The material processing, including BV doping, was funded by the Director, Office of Science, Office of Basic Energy Sciences, Material Sciences and Engineering Division, U.S. Department of Energy, under Contract DE-AC02-05CH11231. Device fabrication and analysis was funded by the NSF E3S Center.

■ REFERENCES

(1) Alam, K.; Lake, R. K. *IEEE Trans. Electron Devices* **2012**, *59*, 3250.
(2) Chhowalla, M.; Shin, H. S.; Eda, G.; Li, L. J.; Loh, K. P.; Zhang, H. *Nat. Chem.* **2013**, *5*, 263.
(3) Geim, A. K.; Grigorieva, I. V. *Nature* **2013**, *499*, 419.
(4) Butler, S. Z.; Hollen, S. M.; Cao, L. Y.; Cui, Y.; Gupta, J. A.; Gutiérrez, H. R.; Heinz, T. F.; Hong, S. S.; Huang, J.; Ismach, A. F.; Johnston-Halperin, E.; Kuno, M.; Plashnitsa, V. V.; Robinson, R. D.; Ruoff, R. S.; Salahuddin, S.; Shan, J.; Shi, L.; Spencer, M. G.; Terrones, M.; Windl, W.; Goldberger, J. E. *ACS Nano* **2013**, *7*, 2898.
(5) Fontana, M.; Deppe, T.; Boyd, A. K.; Rinzan, M.; Liu, A. Y.; Paranjape, M.; Barbara, P. *Sci. Rep.* **2013**, *3*, No. 1634.
(6) Radisavljevic, B.; Radenovic, A.; Brivio, J.; Giacometti, V.; Kis, A. *Nat. Nanotechnol.* **2011**, *6*, 147.
(7) Yoon, Y.; Ganapathi, K.; Salahuddin, S. *Nano Lett.* **2011**, *11*, 3768.
(8) Huang, X.; Zeng, Z. Y.; Zhang, H. *Chem. Soc. Rev.* **2013**, *42*, 1934.
(9) Mak, K. F.; Lee, C.; Hone, J.; Shan, J.; Heinz, T. F. *Phys. Rev. Lett.* **2010**, *105*, No. 136805.
(10) Chen, M. K.; Nam, H.; Wi, S. J.; Ji, L.; Ren, X.; Bian, L. F.; Lu, S. L.; Liang, X. G. *Appl. Phys. Lett.* **2013**, *103*, No. 142110.
(11) Fang, H.; Chuang, S.; Chang, T. C.; Takei, K.; Takahashi, T.; Javey, A. *Nano Lett.* **2012**, *12*, 3788.
(12) Fang, H.; Tosun, M.; Seol, G.; Chang, T. C.; Takei, K.; Guo, J.; Javey, A. *Nano Lett.* **2013**, *13*, 1991.
(13) Chen, W.; Qi, D.; Gao, X.; Wee, A. T. S. *Prog. Surf. Sci.* **2009**, *84*, 279.
(14) Gao, Y.; Yip, H. L.; Chen, K. S.; O'Malley, K. M.; Acton, O.; Sun, Y.; Ting, G.; Chen, H.; Jen, A. K. Y. *Adv. Mater.* **2011**, *23*, 1903.
(15) *Carbon Nanotube Electronics*; Javey, A., Kong, J., Eds.; Springer: New York, 2009.
(16) Lv, R. T.; Terrones, M. *Mater. Lett.* **2012**, *78*, 209.
(17) Takei, K.; Kapadia, R.; Li, Y. J.; Plis, E.; Krishna, S.; Javey, A. *J. Phys. Chem. C* **2013**, *117*, 17845.
(18) Yu, W. J.; Liao, L.; Chae, S. H.; Lee, Y. H.; Duan, X. *Nano Lett.* **2011**, *11*, 4759.
(19) Kim, S. M.; Jang, J. H.; Kim, K. K.; Park, H. K.; Bae, J. J.; Yu, W. J.; Lee, I. H.; Kim, G.; Loc, D. D.; Kim, U. J.; Lee, E. H.; Shin, H. J.; Choi, J. Y.; Lee, Y. H. *J. Am. Chem. Soc.* **2009**, *131*, 327.
(20) Montalti, M.; Credi, A.; Prodi, L.; Gandolfi, M. T. *Handbook of Photochemistry*, 3rd ed.; CRC Press: Boca Raton, FL, 2006.
(21) Hernández-Alonso, M. D.; Fresno, F.; Suárez, S.; Coronado, J. M. *Energy Environ. Sci.* **2009**, *2*, 1231.
(22) Schlaf, R.; Lang, O.; Pettenkofer, C.; Jaegermann, W. *J. Appl. Phys.* **1999**, *85*, 2732.
(23) *CRC Handbook of Chemistry and Physics*, 94th ed.; CRC Press: Boca Raton, FL, 2013.
(24) Chakraborty, B.; Bera, A.; Muthu, D. V. S.; Bhowmick, S.; Waghmare, U. V.; Sood, A. K. *Phys. Rev. B* **2012**, *85*, No. 161403.
(25) Kaasbjerg, K.; Thygesen, K. S.; Jacobsen, K. W. *Phys. Rev. B* **2012**, *85*, No. 115317.
(26) Radisavljevic, B.; Kis, A. *Nat. Mater.* **2013**, *12*, 815.

Supporting Information

Air-stable surface charge transfer doping of MoS_2 by benzyl viologen

Daisuke Kiriya[†,‡,ǁ], Mahmut Tosun[†,‡,ǁ], Peida Zhao[†,‡,ǁ], Jeong Seuk Kang[†,‡] and Ali Javey[†,‡,ǁ,*]

[†]*Electrical Engineering and Computer Sciences, University of California at Berkeley, Berkeley, California 94720, United States*

[‡]*Materials Sciences Division, Lawrence Berkeley National Laboratory, Berkeley, California 94720, United States*

[ǁ]*Berkeley Sensor and Actuator Center, University of California, Berkeley, California 94720, United States*

* ajavey@berkeley.edu

Synthesis of BV molecule and doping method

The preparation of the BV solution is done via the method described in reference (ref.19 in manuscript). Briefly, benzyl viologen dichloride (5~25 mg, Sigma-Aldrich) was dissolved into Milli-Q water (5 ml) followed by adding toluene (5 ml) to make a bilayer. Sodium borohydride (~3.7 g, Sigma-Aldrich) was added to the water/toluene bilayer solution which was then kept for one day. The top toluene layer was then extracted and used for doping. The MoS_2 doping was performed by either drop-casting the BV solution onto the device substrate or immersion of the device substrate into the BV solution for 12 hours. Both approaches gave similar results. After that, N_2 gas was then used to remove extra amount of molecule and solvent.

Fabrication of the devices

All devices are fabricated with standard lithographic techniques using S1818 photoresist for photolithography (for devices shown in Fig. 2d an Fig. S1b) and PMMA for electron beam lithography. The gate oxide of the top gated device consists of a 1 nm thick SiO_x layer deposited via electron beam evaporation followed by a 20 nm thick ZrO_2 layer deposited via atomic layer deposition at 110 °C (Cambridge Nano Tech). The SiO_x layer was used as a nucleation layer for ALD of ZrO_2. The gate-stack was made by electron beam lithography, deposition of SiO_x/ZrO_2 gate dielectric, evaporation of the metal gate, followed by the lift-off of the entire gate stack in acetone. Source, drain, and gate metals were all deposited via electron beam evaporation.

Characterization

Microscope images were taken using an Olympus BX51 microscope equipped with a digital camera (Olympus, QCOLOR3). All electrical characterizations were carried out with an HP 4155C analyzer with a probe station. The low temperature electrical characterization was carried out with cryogenic probe station (Lake Shore) with a Lake Shore 332 temperature controller. Raman spectroscopy was conducted with HORIBA LabRAM HR800. We used 532 nm excitation wavelength and 10 sec exposure (two integration times) for the measurement shown in Figure 2c.

Temperature dependency of the I_{DS}-V_{GS} for the BV doped device

In addition to testing in an ambient environment shown in Figures 2 and 3, the electronic properties of the BV-doped MoS_2 were also explored in vacuum and at low temperatures. A small increase in the current was observed after placing the sample under vacuum (1×10^{-5} Torr, Fig. S3), which can be attributed to a reduction in the work function of the S/D metal electrodes (Ni/Au) via removal of gases such as O_2. Figure S4a shows the temperature dependence of the transfer curves under high vacuum. A monotonic increase of the on-current level is observed as the temperature was decreased for the BV doped sample (Fig. S4a). Figure S4b shows the temperature dependence of the transconductance calculated from V_G = 20 to 40 V; the transconductance increases as the temperature is decreased from 297 to 100 K. For Schottky contacted devices, the current injection over the Schottky barrier (SB, thermionic emission in Fig. S4c) at the source decreases at lower

temperatures. This was previously observed in undoped TMDC devices, which is indicative of the SB nature of the devices, suggesting that the current of the device is limited by the contact resistance and not the channel resistance. The BV doped samples, on the other hand, exhibit opposite trend with enhanced conductance at lower temperatures. In our BV doped device, the thermionic emission is not the dominant mechanism of current injection given the thinning of the barrier by degenerate doping of MoS_2 (Fig. S4d). Instead, the current in our device is limited by phonon scattering in the MoS_2 channel which has an inverse relationship to temperature, consistent with the temperature dependent results. The data clearly depicts ohmic contact formation with BV doping.

Supporting Figures

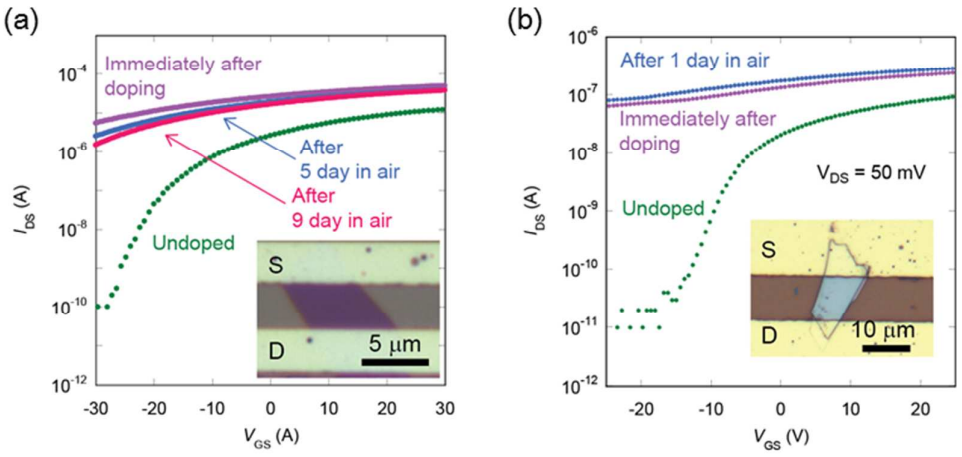

Figure S1. Transfer characteristic curves of a device with a (a) quad-layered flake and (b) a thick MoS_2 flake channel (shown in the inset picture, thickness of the flake is ~150 nm) before and after BV-doping. Both devices exhibit effective *n*-doping of MoS_2 by BV coverage. Furthermore, both devices exhibit excellent stability in ambient air.

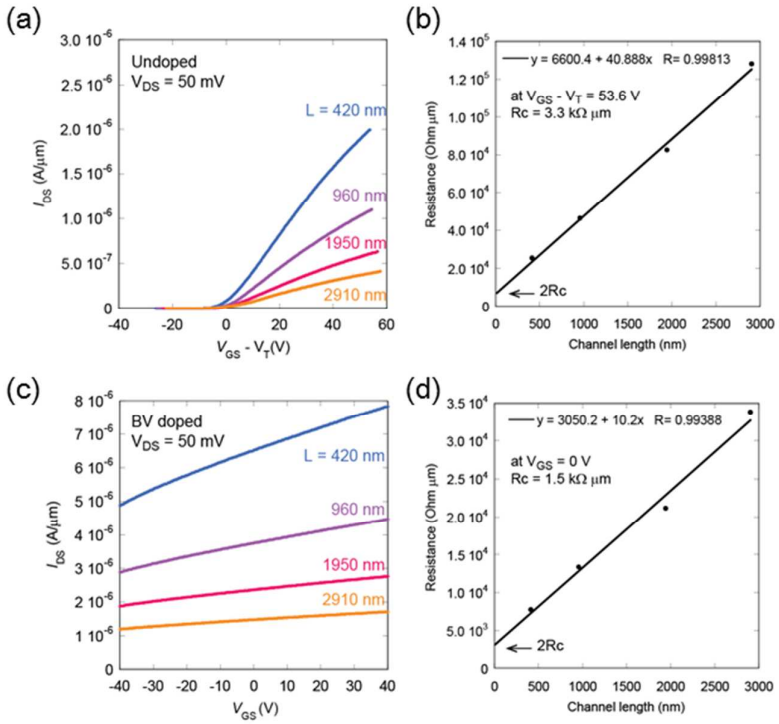

Figure S2. (a) Transfer characteristic curves and (b) resistance versus channel length for a MoS_2 flake with Ni/Au contacts before BV doping (undoped). (c) Transfer characteristic curves and (d) resistance versus channel length at V_{GS} = 0 V for the same MoS_2 after BV doping.

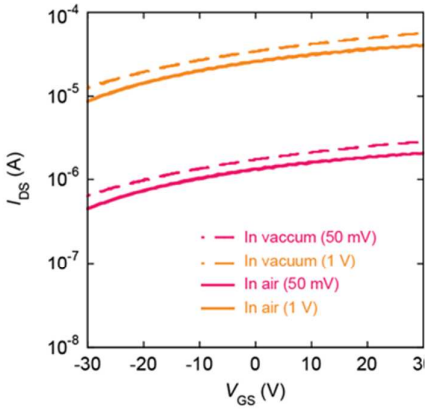

Figure S3 The transfer characteristic curves of a BV-doped MoS_2 sample under high vacuum (1×10^{-5} Torr). Dashed lines are the curves in vacuum and solid lines are in air with V_{DS} = 0.05 (pink) and 1 V (orange).

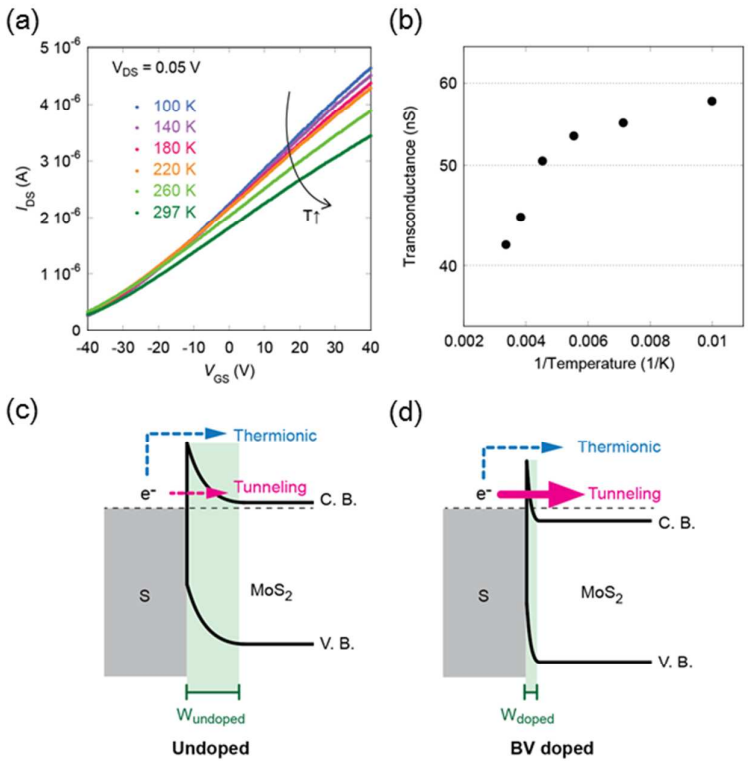

Figure S4 (a) Temperature dependence of the transfer characteristic curves from room temperature (297 K) to 100 K for the same flake shown in Figure 2b. Monotonic increase of the on-current was observed as the temperature was decreased. The applied drain voltage is V_{DS} = 0.05 V. (b) Temperature dependence of the transconductance obtained from the slope of the transfer curves for V_G = 20 to 40. (c) A qualitative energy diagram between Ni/Au metal source (S) and MoS_2 flake for the undoped sample. Tunneling current is low because the Schottky barrier width ($W_{undoped}$) is thick. (d) A qualitative energy diagram for the BV-doped MoS_2 sample. Due to the thin Schottky width (W_{doped}), electrons can tunnel directly through the barrier, resulting in ohmic contact formation.

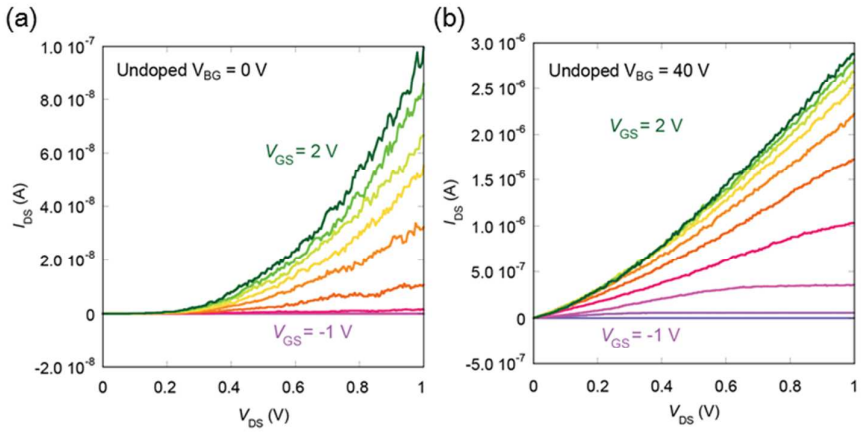

Figure S5. Output characteristic curves of the top-gated MoS_2 device shown in Figure 4 of the main text before BV doping (a) with the back-gate grounded (V_{BG} = 0 V) and (b) with a back gate voltage of V_{BG} = 40 V. Output curves are measured in 0.3 V increments.

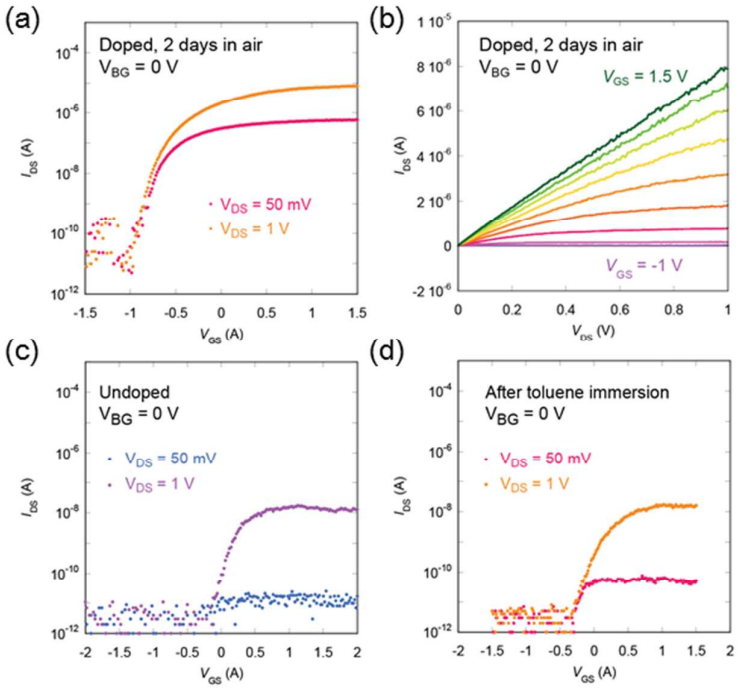

Figure S6 (a) Transfer characteristic curves of the top-gated FET with BV-doped (n^+) source/drain contacts after keeping in air for 2 days. (b) Output characteristic curves of the device shown in (a). The top gate bias was applied in 0.25 V increments. (c) Transfer characteristic curves of the top gate device before BV doping and (d) after toluene immersion of the BV-doped device to remove BV dopant under V_{DS} = 50 mV (blue and pink) and 1 V (purple and orange).